

## AVA MIGRATION AND MULTISCALE CHARACTERIZATION IN FINELY LAYERED MEDIA

KES WAPENAAR, WIM VAN GELOVEN, JEROEN GOUDSWAARD, AART-JAN VAN WIJNGAARDEN and FRANK DESSING

*Centre for Technical Geoscience, Laboratory of Seismics and Acoustics, Delft University of Technology, P.O. Box 5046, 2600 GA Delft, The Netherlands.*

(Received JUNE 10, 1997; revised version accepted July 17, 1997)

### ABSTRACT

Wapenaar, C.P.A., van Geloven, W.J.F., Goudswaard, J.C.M., van Wijngaarden, A.-J. and Dessing, F.J., 1997. AVA migration and multiscale characterization in finely layered media. *In: Hubral, P. (Ed.), Amplitude-Preserving Seismic Reflection Imaging. Journal of Seismic Exploration*, 6: 181-198.

The fine-layering of the earth's subsurface causes apparent amplitude-versus-angle (AVA) effects in seismic reflection data. One can distinguish between propagation- and reflection-related apparent AVA effects: propagation through finely layered media causes angle-dependent wavelet *dispersion*, whereas the reflection of a package of thin layers is accompanied by angle-dependent wavelet *interference*. Obviously, both types of apparent AVA effects hamper AVA inversion for the medium parameters.

In migration, the propagation-related dispersion effects can be compensated for in the downward extrapolation process by means of inverse generalized primary propagators. The reflection-related interference effects can be equalized for all propagation angles by applying an angle-dependent filter in the imaging step.

Angle-dependent migration, including the above-mentioned modifications, yields an angle-dependent reflectivity section in which the apparent AVA effects of fine-layering are suppressed. This type of section may serve as input for local AVA inversion as well as for multiscale characterization by means of the wavelet transform. The latter process yields information about the local scaling exponents of composite reflectors in the earth's subsurface.

KEY WORDS: fine-layering, dispersion, interference, angle-dependent, multiscale, singularities.

## INTRODUCTION

The reflection information in seismic measurements is blurred by the propagation effects between the surface and the reflecting boundaries in the subsurface. In seismic migration one aims to image the reflection properties by eliminating the propagation effects from the seismic measurements. These propagation effects are generally quantified in terms of one-way wavefield propagators in a macro model (Berkhout, 1982). Consequently, the elimination of the propagation effects is accomplished by applying the inverse of these wavefield propagators to the seismic data. For macro models with small contrasts, the inverse propagators are well approximated by the complex conjugate of the forward propagators.

Extensive studies on wave propagation through 1-D finely layered media have shown that internal multiple scattering may seriously affect the propagation properties of the seismic wavefield [see e.g., O'Doherty and Anstey (1971); Hubral et al. (1980); Resnick et al. (1986); Ursin (1987); Herrmann and Wapenaar (1992); Stanke and Burridge (1993); Shapiro et al. (1994)]. The main effect is an angle-dependent dispersion. Current macro models do not account for this effect. Consequently, this effect is also ignored in migration. This may result in dispersed images and erroneous amplitude-versus-angle (AVA) effects. Apart from these propagation related distortions, the interference of the reflection responses of 'reflector packages' in finely layered media causes apparent AVA effects as well.

In this paper we discuss a migration approach that accounts for the propagation-related (dispersion) as well as for the reflection-related (interference) apparent AVA effects of fine-layering. With the aid of some examples, we show how this improves the post-migration AVA results. Moreover, we discuss a multiscale analysis of these AVA results and show that relevant information can be retrieved about the local scaling exponents of composite reflectors in the earth's subsurface.

## THE GENERALIZED PRIMARY REPRESENTATION

In order to account for the effects of fine-layering in migration, a 3-D *generalized primary* representation of seismic reflection data has been developed (Wapenaar, 1996). The notion 'generalized primary' was introduced by Hubral et al. (1980) and Resnick et al. (1986), who used this term for reflection data from 1-D finely layered media. For 3-D finely layered media, the generalized primary representation reads (in the frequency ( $\omega$ ) domain)

$$P^-(\mathbf{x}_R, \mathbf{x}_S, \omega) = \int W_g^-(\mathbf{x}_R, \mathbf{x}, \omega) \hat{R}(\mathbf{x}, \omega) W_g^+(\mathbf{x}, \mathbf{x}_S, \omega) S^+(\mathbf{x}_S, \omega) d^3\mathbf{x} \quad , \quad (1)$$

where, from right to left,  $S^+(\mathbf{x}_S, \omega)$  represents the source for downgoing waves at the source point  $\mathbf{x}_S = (x_S, y_S, z_S)$ ,  $W_g^+(\mathbf{x}, \mathbf{x}_S, \omega)$  describes generalized downward propagation (including internal multiple scattering) into the subsurface,  $\hat{R}(\mathbf{x}, \omega)$  is a pseudo-differential operator that describes reflection at any point  $\mathbf{x} = (x, y, z)$  in the subsurface,  $W_g^-(\mathbf{x}_R, \mathbf{x}, \omega)$  describes generalized upward propagation to the surface and  $P^-(\mathbf{x}_R, \mathbf{x}_S, \omega)$  represents the upgoing wave field at the receiver point  $\mathbf{x}_R = (x_R, y_R, z_R)$ , see Fig. 1. Note that equation (1) does not account for surface-related multiples. In the following we shall assume that decomposition and surface-related multiple elimination (e.g., Verschuur et al., 1992) has been carried out.

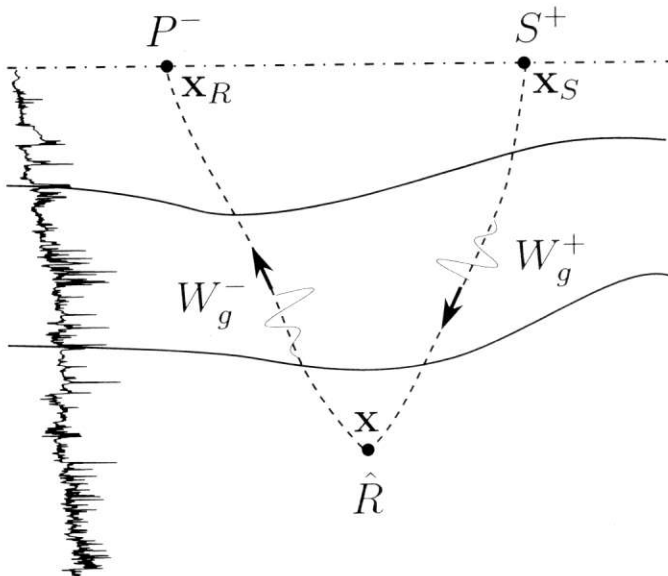


Fig. 1. The generalized primary representation for 3-D finely layered media. The dispersion included in the propagators  $W_g^+$  and  $W_g^-$  accounts for the 'propagation related' apparent AVA effects in the reflection response  $P^-$ .

#### GENERALIZED AVA MIGRATION

In essence, migration based on the generalized primary representation is accomplished by applying the inverse versions of the propagators  $W_g^+$  and  $W_g^-$  to the data  $P^-$ , thus resolving the reflectivity operator  $\hat{R}$ . For finely layered media, the inverse propagators cannot be approximated by the complex conjugate forward propagators. Correction operators are required that compensate for the transmission losses. Using reciprocity, these transmission losses, and hence the correction operators, can be estimated from the

multi-dimensional cross-correlation of the reflection measurements at the surface. The inverse propagators that are thus constructed compensate for the propagation-related apparent AVA effects of fine-layering [Wapenaar and Herrmann (1993); a slightly different approach was discussed by Widmaier et al. (1996)]. Applying these inverse propagators to the surface data  $P^-(\mathbf{x}_R, \mathbf{x}_S, \omega)$  yields the downward extrapolated data  $P^-(\mathbf{x}', \mathbf{x}, \omega)$  in the subsurface. After applying a Radon transform with respect to the offset measured along a (dipping) reference level, we obtain  $\tilde{P}^-(\mathbf{p}, \mathbf{x}, \omega)$  for any  $\mathbf{x}$  in the subsurface, with the ray-parameter vector defined as  $\mathbf{p} = (p_x, p_y)$ . At each point  $\mathbf{x}$ , imaging could then be carried out by integrating  $\tilde{P}^-(\mathbf{p}, \mathbf{x}, \omega)$  along the available frequency components for all ray-parameters  $\mathbf{p}$ , yielding  $\tilde{R}(\mathbf{p}, \mathbf{x})$ . However, for different ray-parameters (i.e., different angles) and constant frequency, the finely layered medium is observed with different apparent wavelengths (see Fig. 2 for the special case of a horizontally layered medium). Therefore, the interference effects in  $\tilde{R}(\mathbf{p}, \mathbf{x})$  depend on the ray-parameter  $\mathbf{p}$ , which causes apparent AVA effects. This can be cured by taking a  $\mathbf{p}$ -variant  $\omega$ -integration range in the imaging step, in such a way that the apparent wavelength range is constant for all  $\mathbf{p}$ . We define this  $\omega$ -integration range as

$$\omega_1/\cos\bar{\phi}(\mathbf{p}, \mathbf{x}) < \omega < \omega_2/\cos\bar{\phi}(\mathbf{p}, \mathbf{x}) \quad , \quad (2)$$

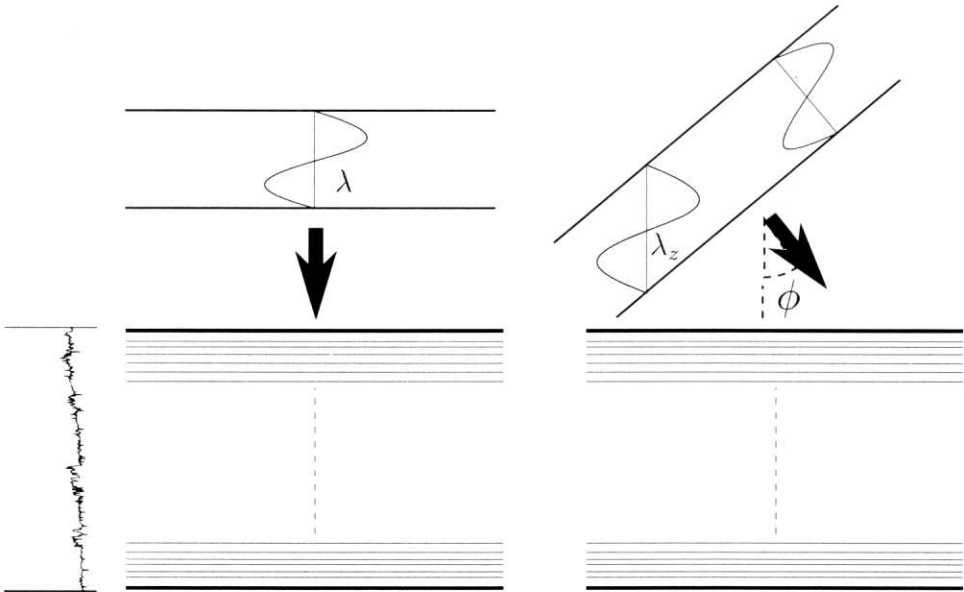


Fig. 2. A finely layered medium that is illuminated at different angles is observed with different apparent wavelengths  $\lambda_z = \lambda/\cos\phi$ . This results in angle-dependent interference, which accounts for the 'reflection related' apparent AVA effects in the reflection response  $P^-$ .

with  $\cos\bar{\phi}(\mathbf{p},\mathbf{x}) = \sqrt{[1 - |\mathbf{p}|^2\bar{c}^2(\mathbf{x})]}$ , where  $\bar{c}(\mathbf{x})$  is the local ‘macro velocity’ and where  $\omega_1$  and  $\omega_2$  can be chosen freely, with the constraint that the range defined in equation (2) should not exceed the band-limits of the source function  $S^+(\mathbf{x}_S,\omega)$ . In this way, the interference effects of reflector packages are not removed but equalized, thus compensating for the reflection-related apparent AVA effects of fine-layering. For a more detailed discussion, see Wapenaar et al. (1995) and for an extension to the elastodynamic situation, see van Geloven et al. (1997). In summary, angle-dependent migration based on the generalized primary representation (‘generalized AVA migration’) involves (1) downward extrapolation using the inverse generalized primary propagators and (2) imaging in the Radon domain, using a  $\mathbf{p}$ -variant  $\omega$ -integration range. Steps (1) and (2) compensate, respectively, for the propagation- and reflection-related apparent AVA effects in the reflection response  $P^-(\mathbf{x}_R,\mathbf{x}_S,\omega)$ , thus yielding an improved AVA reflectivity section  $\bar{R}(\mathbf{p},\mathbf{x})$ .

### Migration example I: horizontally layered medium

In the first example we consider a horizontally layered medium. Fig. 3 shows a velocity log (the density is constant) and the corresponding exact response (modeled with the reflectivity method) in the  $(\mathbf{p},\tau)$ -domain. For this situation, the generalized migration described in the previous section can be carried out entirely in the Radon domain.

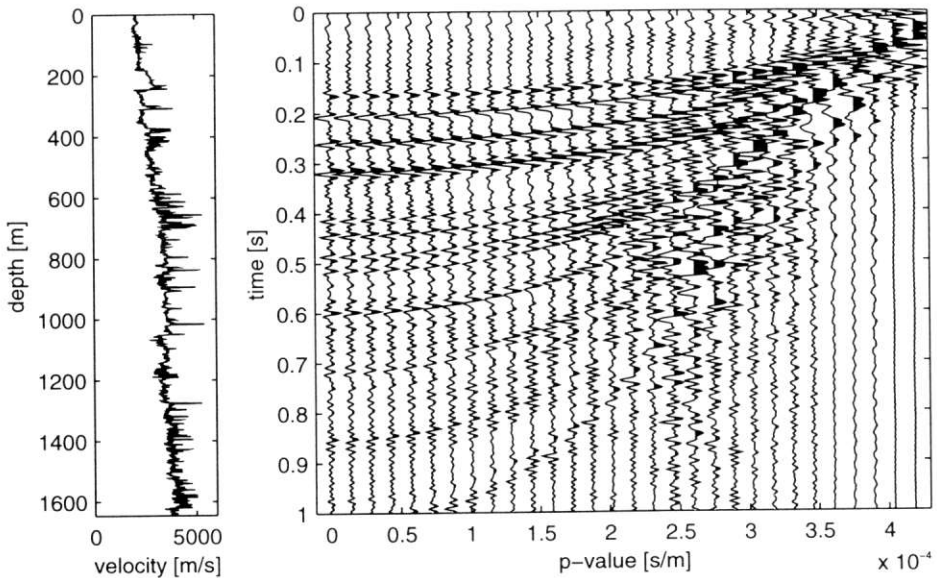


Fig. 3. Velocity log of a horizontally layered medium and the corresponding seismic response in the  $(\mathbf{p},\tau)$ -domain.

The imaged reflectivity  $\tilde{R}(p,z)$  is shown in Fig. 4. In order to analyze the improvements of the generalized migration, we zoom in on the reflection event related to the singularity at  $z = 890$  m. In Fig. 5a we show a reference section (i.e., a bandlimited version of the angle-dependent reflectivity derived directly from the well-log), in Fig. 5b the result of 'normal migration' (i.e., without compensation for the propagation- and reflection-related apparent AVA effects), in Fig. 5c the result of our generalized migration (taken from the section in Fig. 4), in Fig. 5d the picked amplitudes in a small window around at  $z = 890$  m and in Fig. 5e the amplitudes picked exactly at  $z = 890$  m. Note that the generalized migration result (the dashed curves in Figs. 5d and 5e) matches the reference section (the solid curves) much more accurately than the normal migration result (the dotted curves).

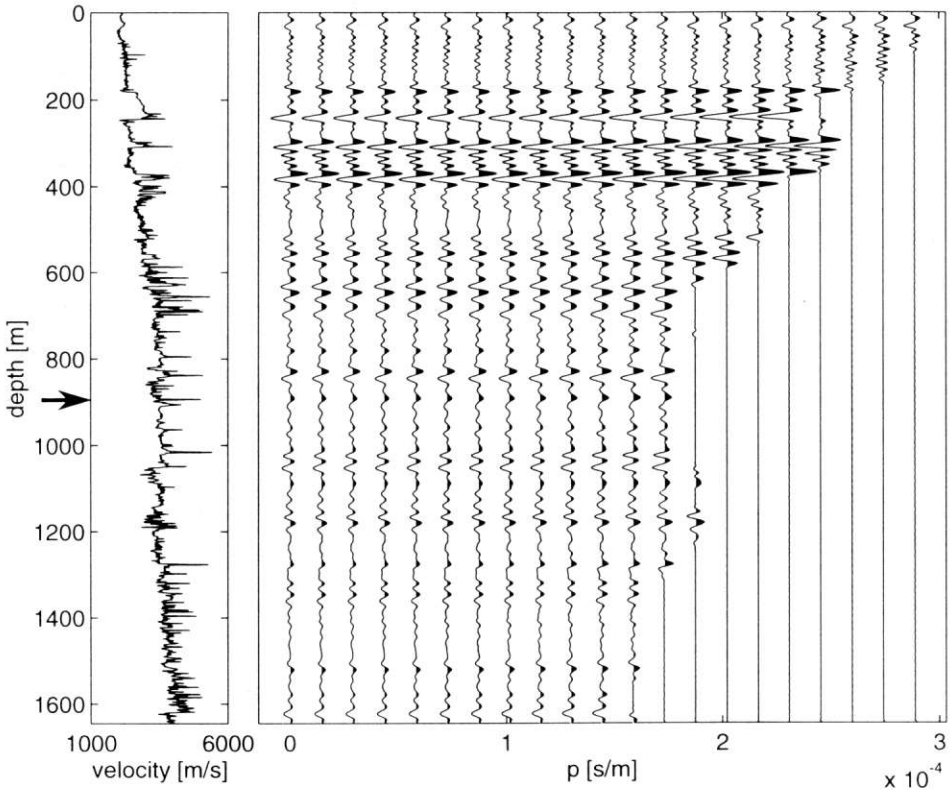


Fig. 4. Migration result  $\tilde{R}(p,z)$ , obtained by applying the inverse versions of the generalized primary propagators (in the ray-parameter domain) and imaging with the equalization filter, defined by equation (2).

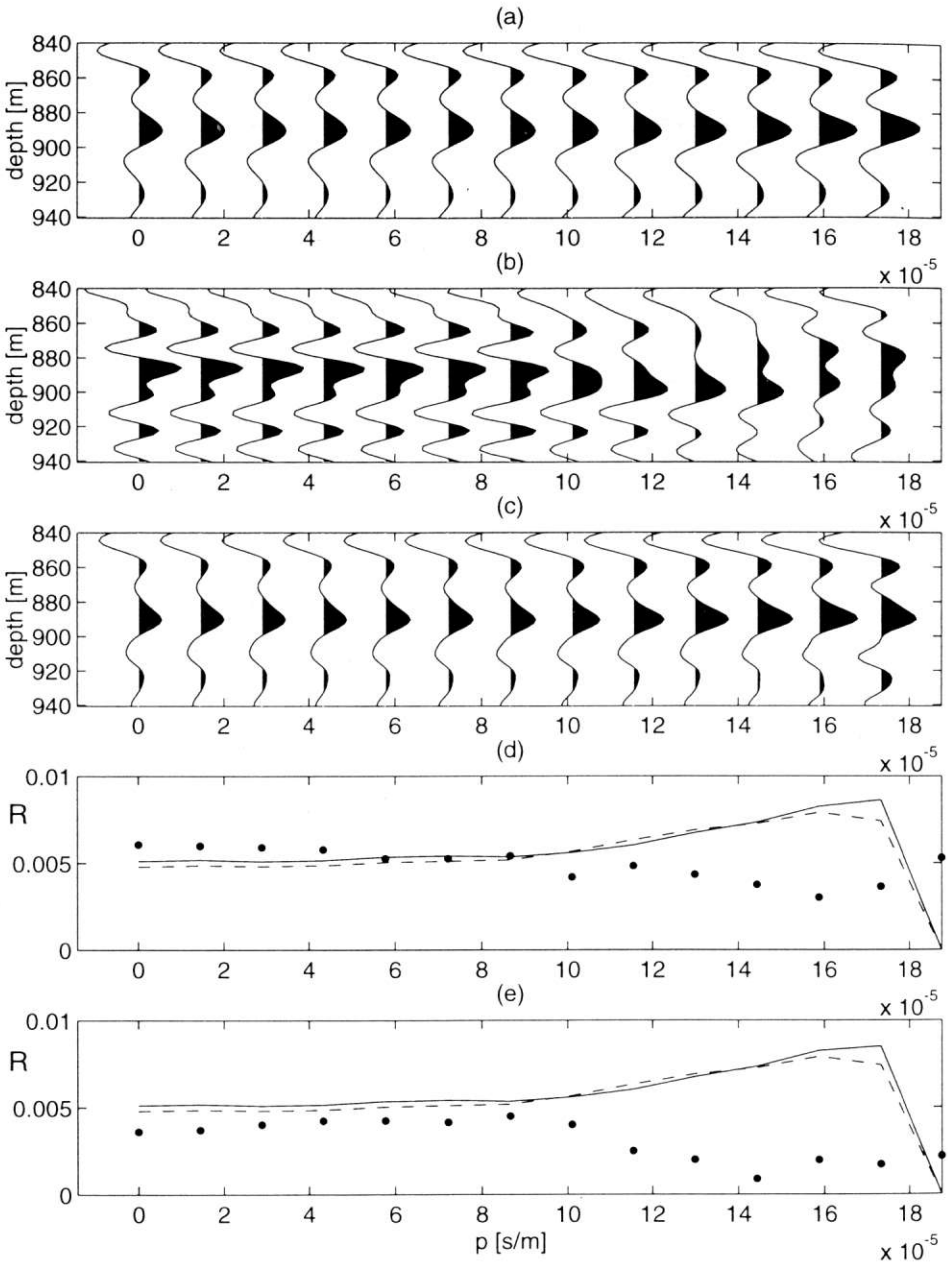


Fig. 5. Reflectivity section around  $z = 890$  m. (a) Reference section. (b) Normal migration result. (c) Generalized migration result. (d) Picked amplitudes in a small depth interval around  $z = 890$  m [solid: (a), dotted: (b), dashed: (c)]. (e) Picked amplitudes exactly at  $z = 890$  m.

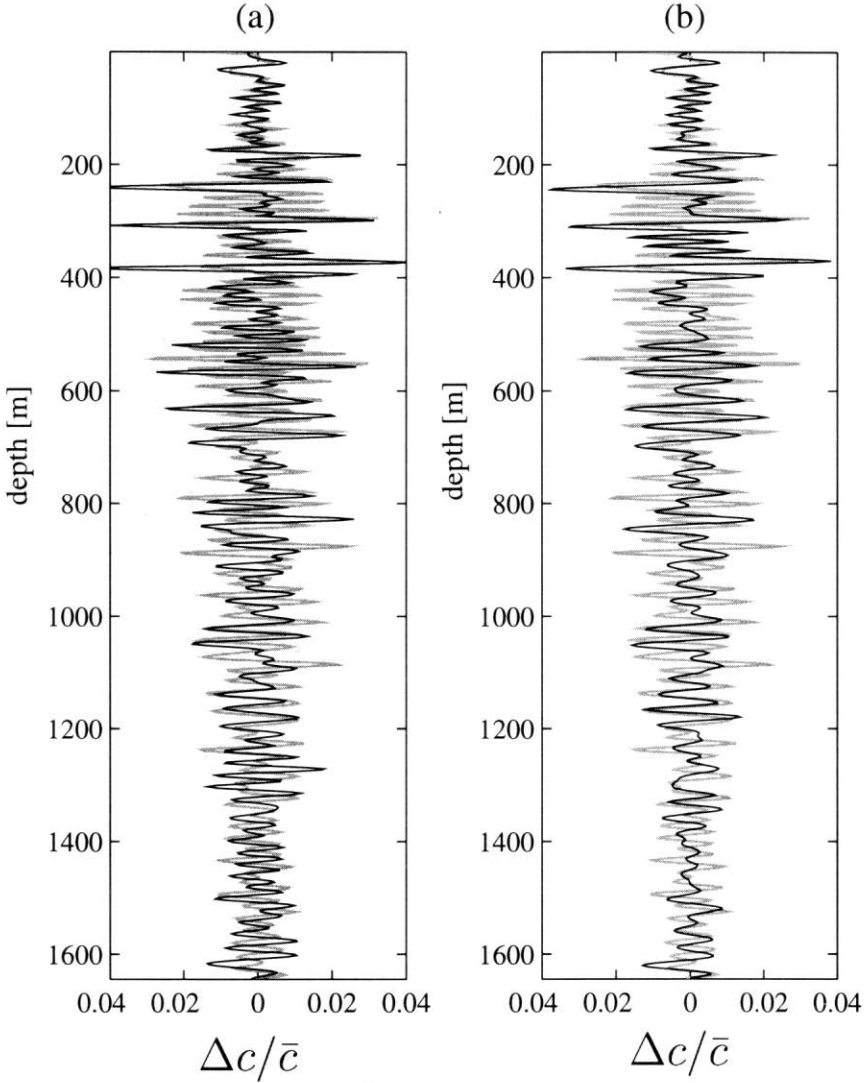


Fig. 6. Local AVA inversion applied to the results of normal migration (a) and generalized migration (b). The grey curves are the inversion results, the black curves are filtered versions of the velocity log.

Obviously, the generalized migration preconditions the data ideally for local AVA inversion [Smith and Gidlow (1987), de Haas and Berkhout (1990), van Wijngaarden and Berkhout (1996), Ursin et al. (1996)]. We applied the method discussed by van Wijngaarden and Berkhout (1996) to the normal as well as to the generalized migration result, aiming for the medium parameter

contrasts  $\Delta c(z)/\bar{c}(z)$  and  $\Delta\rho(z)/\bar{\rho}(z)$  (hence, without presuming that the density  $\rho$  is constant). The resolved functions  $\Delta c(z)/\bar{c}(z)$  obtained after the normal and generalized migration are represented by the grey curves in Figs. 6a and 6b, respectively. The black curves in both figures are appropriately bandfiltered versions of  $\Delta c(z)/\bar{c}(z)$ , obtained directly from the velocity log. Note that the inversion result obtained after generalized migration (Fig. 6b) matches the filtered velocity log quite accurately. Compared with the inversion result obtained after normal migration (Fig. 6a) some resolution has been lost due to the equalization filter, defined by equation (2).

### Migration example II: 2-D inhomogeneous medium

In the second example we consider a 2-D inhomogeneous medium (Fig. 7), which consists of a dipping, finely layered target and a smooth 2-D inhomogeneous overburden (hence, in this example we disregard the propagation-related apparent AVA effects of the overburden). We modeled 400 shot records with a hybrid modeling scheme (wavenumber domain modeling in the target, followed by ray-tracing through the overburden). The results of downward extrapolation and imaging along a single line normal to the target (see Fig. 7) are shown in Fig. 8, zoomed in around  $z' = 155$  m (note that  $z'$  denotes here the 'depth' along the dipping line, with  $z' = 0$  at the top of the target). The modified migration result [i.e., imaging with the equalization filter defined by equation (2)] matches the reference section significantly more accurately than the normal migration result.

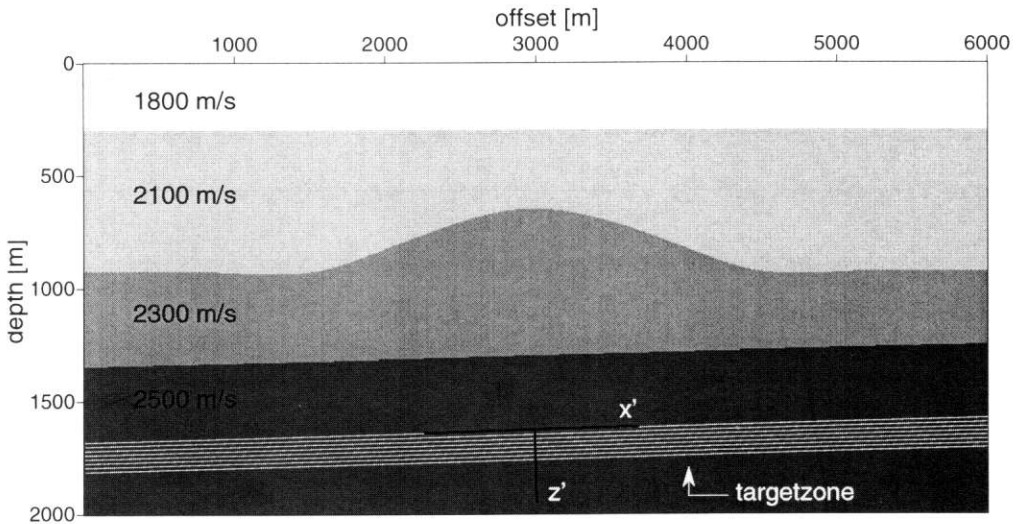


Fig. 7. 2-D inhomogeneous subsurface model.

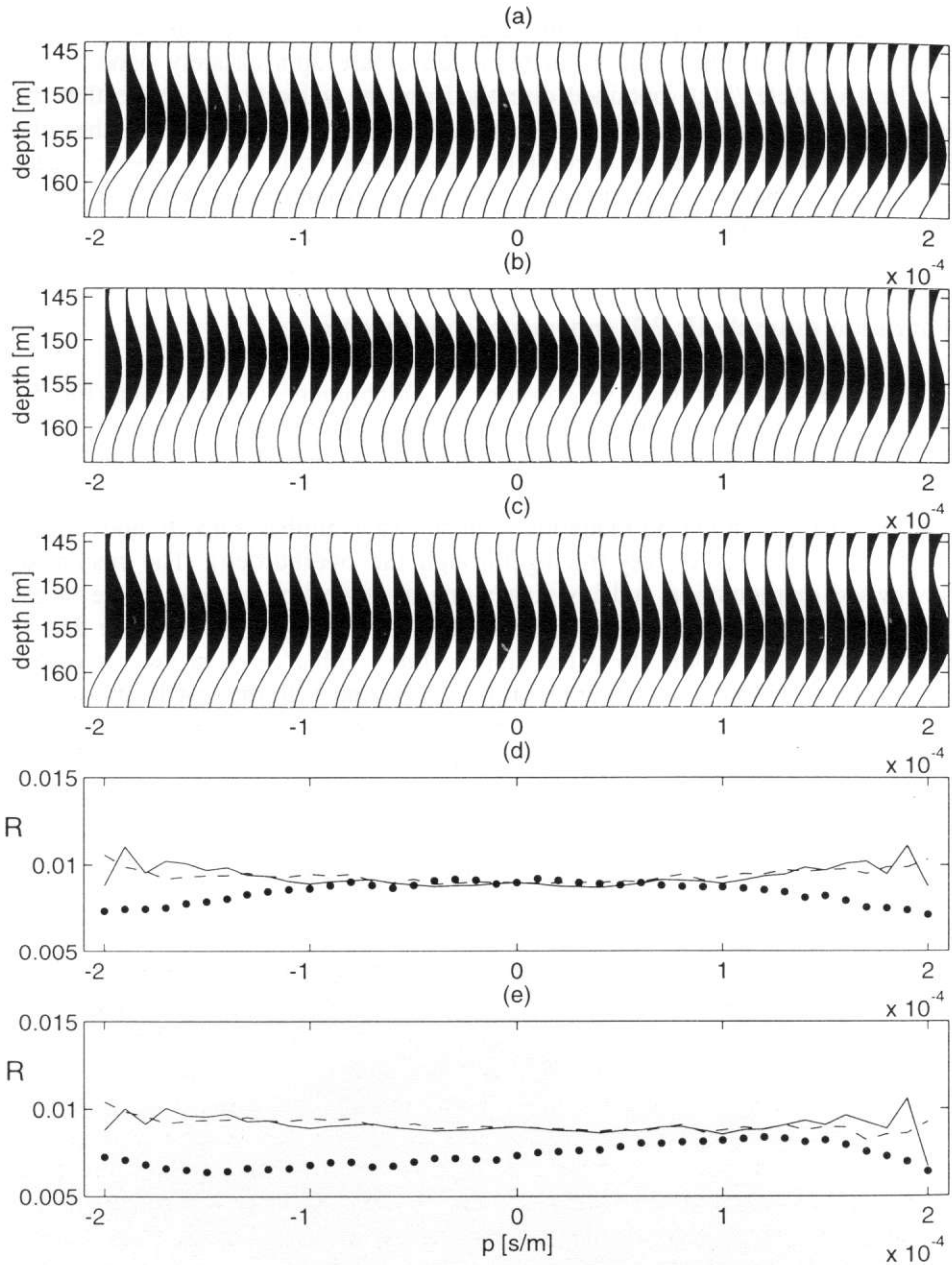


Fig. 8. Reflectivity section around  $z' = 155$  m. (a) Reference section. (b) Normal migration result. (c) Modified migration result. (d) Picked amplitudes in a small depth interval around  $z' = 155$  m [solid: (a), dotted: (b), dashed: (c)]. (e) Picked amplitudes exactly at  $z' = 155$  m.

## MULTISCALE CHARACTERIZATION

Because of the band-limited nature of seismic data, migration and inversion results have a finite resolution, which implies that it is impossible to determine the precise nature of reflectors in the earth's subsurface: at scales well below the seismic wavelength, continuous as well as discontinuous reflector models (step-functions or other singularities) are equally plausible. Seismic data do carry information, however, on the nature of 'composite reflectors' (reflector packages) at scales in the order of the seismic wavelength. In the previous sections we have indicated how to account for the interaction of seismic waves with reflector packages in AVA migration and inversion. In this section we address the following questions:

- \* How can we parameterize composite reflectors in the seismic scale range?
- \* What are their effective reflection properties?
- \* How can we resolve their parameters from the seismic data?

**Multiscale analysis of well-logs**

In order to find a parameterization for the composite reflectors in the seismic scale range, we analyze a well-log, following the procedure proposed by Herrmann (1997). Fig. 9a shows a velocity well-log  $c(z)$  and Fig. 9b the continuous wavelet transform  $\check{c}(\sigma, z)$  of this well-log. In essence, this result has been obtained by convolving the well-log with scaled versions of one and the same analyzing wavelet  $\psi(z)$ , according to

$$\check{c}(\sigma, z) = (1/\sigma) \int_{-\infty}^{\infty} c(z') \psi[(z' - z)/\sigma] dz' \quad , \quad (3)$$

with  $\sigma > 0$ . The different traces in Fig. 9b correspond to different scales. Taking the modulus of the data in Fig. 9b and connecting the local maxima from trace to trace, yields the so-called modulus maxima lines (Mallat and Hwang, 1992) that are shown in Fig. 9c. Fig. 9d shows the amplitudes measured along some of these lines, on a log-log scale. These amplitude-versus-scale graphs are characteristic for the effective singularities in the well-log at the origin of the selected modulus maximum lines (denoted by the arrows in Fig. 9a). Note that the support of these singularities is not confined to a point but to a region: since we used analyzing wavelets in the seismic scale range, these singularities actually represent composite reflectors in the seismic scale range. The graphs in Fig. 9d show that the amplitudes of the singularities are scale-dependent; however, the *slopes* of these graphs are approximately constant. Hence, we can parameterize the scale-dependency of each of the corresponding singularities in Fig. 9a by a single scaling exponent  $\alpha$ .

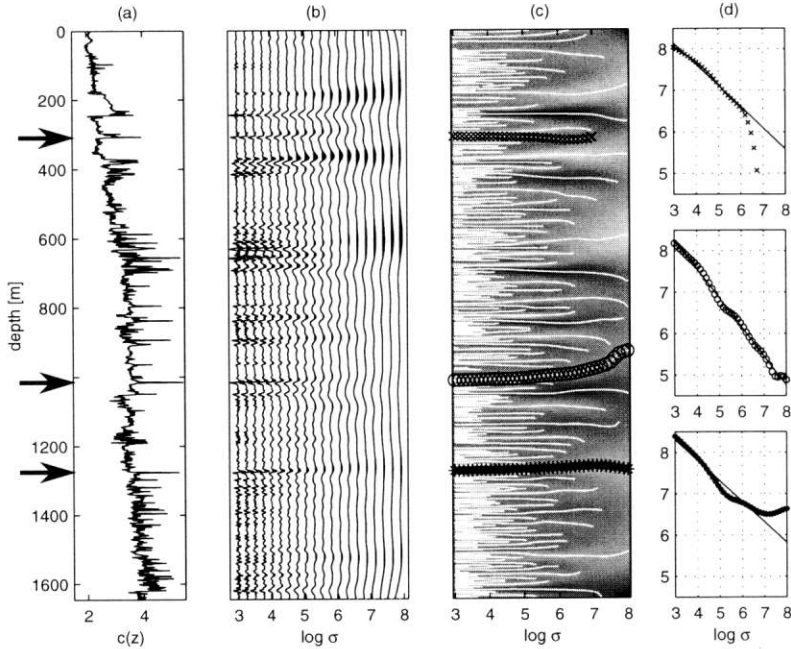


Fig. 9. Multiscale analysis of a well-log (after Herrmann, 1997). (a) The original well-log. (b) The well-log at different scales, obtained by the continuous wavelet transform. Scales  ${}^2\log\sigma = 3$  to  ${}^2\log\sigma = 7$  correspond to the seismic scale range. (c) Modulus maxima lines, obtained from (b). (d) Amplitude-versus-scale graphs, measured along the highlighted modulus maxima lines in (c). The slopes of these graphs define the local scaling exponents ( $\alpha = -0.52, -0.70, -0.50$ ) of the singularities in the well-log (at  $z = 305, 1010, 1270$  m, respectively).

To understand the meaning of the scaling exponent  $\alpha$ , we consider a synthetic well-log, consisting of shifted versions of the singular function

$$c(z) = \begin{cases} c_1 |z/z_1|^\alpha & \text{for } z < 0 \\ c_2 |z/z_2|^\alpha & \text{for } z > 0 \end{cases}, \quad (4)$$

see Fig. 10a. We applied a multiscale analysis (similar to that discussed above) to this synthetic well-log, see Figs. 10b, c, d. Note that the slopes of the amplitude-versus-scale graphs in Fig. 10d are constant, just as in Fig. 9d. Using the *self-similarity* property  $c(\beta z) = \beta^\alpha c(z)$  (for  $\beta > 0$ ), it can be shown that  $\alpha$  in equation (4) defines the slopes of the amplitude-versus-scale graphs in Fig. 10d (Mallat and Hwang, 1992; Holschneider, 1995). For example, the step-function in the synthetic well-log in Fig. 10a is described by equation (4) with  $\alpha = 0$ ; its corresponding amplitude-versus-scale graph in Fig. 10d indeed has a zero slope. In the following sections we will use equation (4) as a parameterization of self-similar composite reflectors.

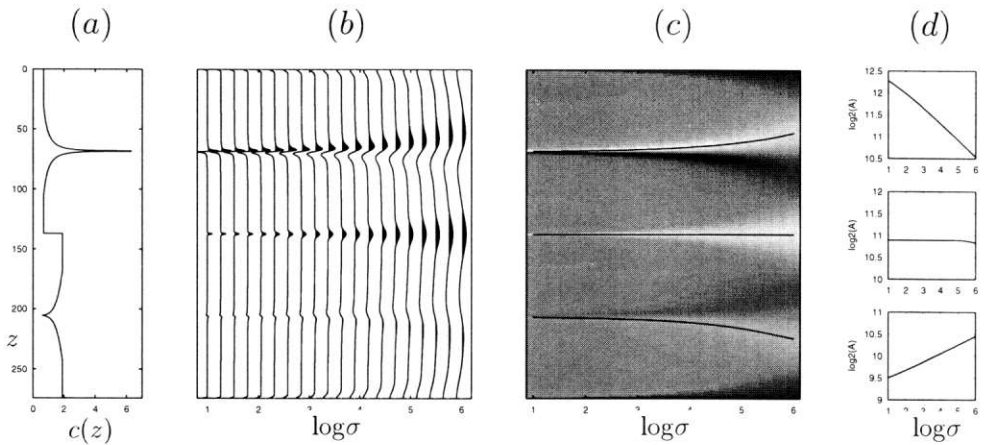


Fig. 10. Multiscale analysis of a synthetic well-log ( $\alpha = -0.4, 0.0, 0.2$ ).

**AVA behaviour of self-similar reflectors**

First we analyze the AVA behaviour of self-similar reflectors, described by equation (4), with numerical experiments. Using the reflectivity method, we modeled the reflection response of two self-similar reflectors, with  $\alpha = 0$  and  $\alpha = -0.4$ , respectively (the other parameters were chosen the same in both cases:  $c_1 = 2000$  m/s,  $c_2 = 3000$  m/s and  $z_1 = z_2 = 10$  m). The reflection amplitudes as a function of ray-parameter  $p$  and frequency  $f$  are shown in Fig. 11. For  $\alpha = 0$  (i.e. for a step-function) these amplitudes appear to be frequency independent (as expected); as a function of the ray-parameter they exhibit the well-known precritical ( $p < 1/c_2$ ) and postcritical ( $p > 1/c_2$ ) behaviour. For  $\alpha = -0.4$  the amplitudes appear to depend on the frequency as well as the ray-parameter. Fig. 12 shows contours of constant amplitude, obtained from Fig. 11.

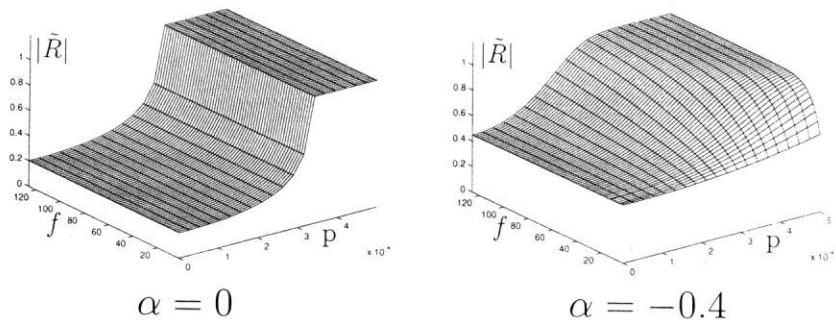


Fig. 11. Angle- and frequency-dependent reflection coefficients for self-similar reflectors, defined by equation (4). (Note that  $p = \sin\phi/c_1$ ;  $f = \omega/2\pi$ ).

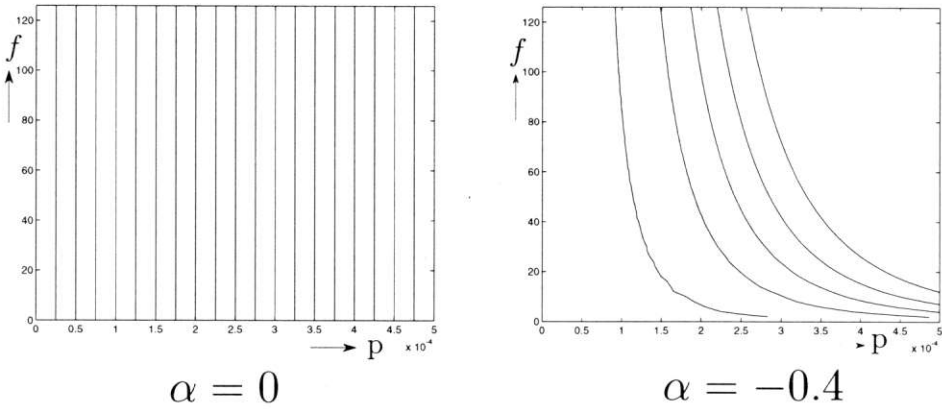


Fig. 12. Contours of constant amplitudes in Fig. 11.

By analyzing the wave equation and boundary conditions in the ray-parameter-frequency domain, using the self-similarity property  $c(\beta z) = \beta^\alpha c(z)$ , it can be shown that for  $\alpha < 1/2$  the reflection coefficient obeys the following self-similarity relation

$$\tilde{R}(p, \omega, z_0) = \tilde{R}(\beta^\alpha p, \beta^{1-\alpha} \omega, z_0) \tag{5}$$

(Wapenaar, 1997). The latter equation implies that  $\tilde{R}(p, \omega, z_0)$  is constant along curves described by

$$p^{1-\alpha} \omega^{-\alpha} = \text{constant} \tag{6}$$

Equation (6) explains the numerically obtained contours in Fig. 12. It clearly shows the effect of the scaling parameter  $\alpha$  on the angle- and frequency-dependent reflection coefficient.

### Multiscale analysis of seismic data

In migration it is usually assumed that reflection coefficients are frequency independent. Figs. 11 and 12 in the previous subsection, however, show that this assumption breaks down for composite reflectors. Hence, in order to retrieve the parameter  $\alpha$  from the seismic data, one would like to extend a migrated section with an extra ‘frequency-axis’. Since the frequency-dependency can be different at each depth, the appropriate way to obtain this ‘frequency-axis’ is by applying a wavelet transform to the migrated data along the depth coordinate (bear in mind that the scale parameter  $\sigma$  is proportional to

the reciprocal local frequency). This idea was first proposed by Dessing et al. (1996), who used this method for multiscale edge detection. Here we pay particular attention to the AVA effects. Obviously the AVA information should be handled with the same care as in the previous sections. Therefore, the proposed wavelet transform should be applied to migration results, obtained with the generalized AVA migration scheme.

We applied the wavelet transform along the depth coordinate to the generalized migration result of Fig. 4, see Fig. 13. Note that a  $(p, \sigma)$ -plane for any depth  $z$  contains the *local* angle- and ‘frequency’-dependent reflection information. To get a stable result, the highlighted  $(p, \sigma)$ -plane in Fig. 13 is not defined at a constant depth but it follows the maximum amplitudes along the  $\sigma$ -direction, similarly to the modulus maxima lines in Figs. 9c and 10c. Using the property  $\sigma \propto 1/\omega$ , it easily follows from equation (6) that the contours in this modulus maxima plane are approximately described by

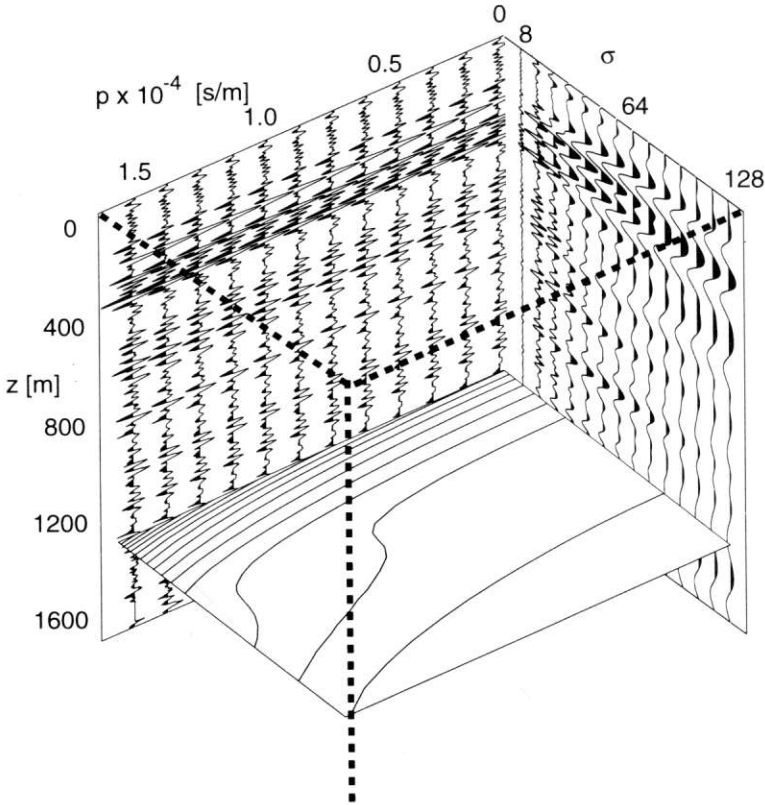


Fig. 13. Wavelet transform of the generalized migration result of Fig. 4. Only two side-planes are shown as well as a modulus maxima plane (with amplitude contours) for the singularity at  $z = 1270$  m. This modulus maxima plane is shown again in Fig. 14c.

$$p^{1-\alpha}\sigma^\alpha = \text{constant} \quad (7)$$

Hence, the local scaling exponent  $\alpha$  can be determined by analyzing these contours.

Fig. 14 shows the contours in the modulus maxima planes retrieved from Fig. 13, for the same singularities that were analyzed in Fig. 9. Using equation (7), we derived from these contours  $\alpha \approx -0.56, -0.85, -0.59$ , respectively. These values correspond neatly to the values  $\alpha = -0.52, -0.70, -0.50$  that we obtained directly from the well-log for the scales that correspond to the seismic scale range (see Fig. 9). For more examples, see Goudswaard et al. (1997).

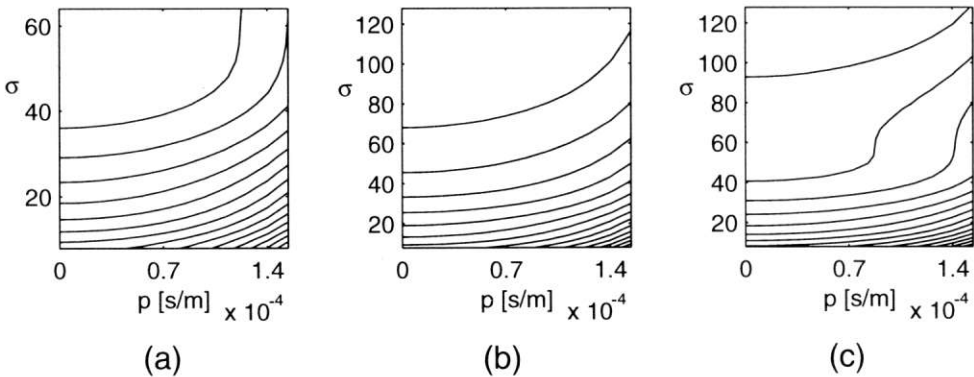


Fig. 14. Contours in the modulus maxima planes (retrieved from Fig. 13) for the singularities at  $z = 305, 1010, 1270$  m (Figs. a, b, c, respectively). The contours are approximately described by equation (7), with  $\alpha \approx -0.56, -0.85, -0.59$ , respectively.

## CONCLUSIONS

### Generalized AVA migration

The *apparent* AVA effects due to fine-layering can be subdivided into propagation- and reflection-related effects.

#### *Propagation-related apparent AVA effects*

The propagation through a package of thin layers is accompanied by wavelet *dispersion*. This dispersion is caused by internal multiple scattering and depends on the propagation angle. It is quantified by the generalized primary propagator. The inverse of this generalized primary propagator can be used in the downward extrapolation step in migration.

### *Reflection related apparent AVA effects*

The reflection of a package of thin layers is accompanied by wavelet *interference*. Since, for a given frequency, the apparent wavelength varies with the angle of incidence, the interference effects are also angle-dependent. Due to the band-limitation of seismic data, the interference effects cannot be removed. We have proposed a filter that *equalizes* these effects. This filter can be integrated in the imaging step in migration.

We have shown, with numerical examples, that migration with the two modifications discussed above yields band-limited reflectivity sections in which the apparent AVA effects of fine-layering are suppressed. From this type of AVA reflectivity sections, the band-limited medium parameter contrasts can be resolved by local AVA inversion.

### **Multiscale characterization**

By applying a multiscale analysis on a well-log (Herrmann, 1997), we have shown that the amplitudes of 'composite reflectors' (reflector packages) are scale-dependent; the slopes  $\alpha$  of the amplitude-versus-scale graphs are often approximately constant (note that  $\alpha = 0$  for step-functions). This implies that these composite reflectors may be parameterized by self-similar singularities, which obey  $c(\beta z) = \beta^\alpha c(z)$ . The angle- and frequency-dependent reflection coefficient of this type of singularities appears to be self-similar as well: it is constant along curves defined by  $p^{1-\alpha}\omega^{-\alpha} = \text{constant}$  or, in the ray-parameter-scale domain,  $p^{1-\alpha}\sigma^\alpha = \text{constant}$ . The latter curves can be analyzed after applying a multiscale analysis to the AVA reflectivity sections, obtained with the generalized migration procedure described above. Using a numerical example, we have shown that the local scaling exponents  $\alpha$  that are thus obtained from the seismic data are consistent with the values that were obtained by the multiscale analysis of the well-log in the seismic scale range. The singularity exponent  $\alpha$  may prove to be a useful seismic indicator. Current research involves the investigation of more general composite reflector models, so that the 'constant slope' assumption can be relaxed.

### ACKNOWLEDGEMENT

The authors would like to thank the Dutch Technology Foundation (STW) and the sponsors of the Delphi consortium for their financial support.

## REFERENCES

- Berkhout, A.J., 1982. Seismic Migration. Imaging of acoustic energy by wave field extrapolation. Elsevier Science Publishers, Amsterdam.
- de Haas, J.C. and Berkhout, A.J., 1990. Local inversion of PP, PS, SP and SS reflections. Expanded Abstr., 60th Ann. Internat. SEG Mtg., San Francisco: 1189-1192.
- Dessing, F.J., Hoekstra, E.V., Herrmann, F.J. and Wapenaar, C.P.A., 1996. Multiscale edge detection by means of multiscale migration. Expanded Abstr., 66th Ann. Internat. SEG Mtg., Denver: 459-462.
- Goudswaard, J.C.M. and Wapenaar, C.P.A., 1997. Resolving well-log singularities from seismic data. Expanded Abstr., 67th Ann. Internat. SEG Mtg., Dallas, in press.
- Herrmann, F.J. and Wapenaar, C.P.A., 1992. Macro description of fine layering: A proposal for an extended macro model. Expanded Abstr., 62nd Ann. Internat. SEG Mtg., New Orleans: 1263-1266.
- Herrmann, F.J., 1997. A Scaling Medium Representation. Ph.D. thesis, Delft University of Technology.
- Holschneider, M., 1995. Wavelets: an Analysis Tool. Oxford University Press, Oxford.
- Hubral, P., Treitel, S. and Gutowski, P.R., 1980. A sum autoregressive formula for the reflection response. Geophysics, 45: 1697-1705.
- Mallat, S.G. and Hwang, W.L., 1992. Singularity detection and processing with wavelets. IEEE Trans. Inform. Theory, 38: 617-643.
- O'Doherty, R.F. and Anstey, N.A., 1971. Reflections on amplitudes. Geophys. Prosp., 19: 430-458.
- Resnick, J.R., Lerche, I. and Shuey, R.T., 1986. Reflection, transmission, and the generalized primary wave. Geoph. J. R. Astr. Soc., 87: 349-377.
- Shapiro, S.A., Hubral, P. and Zien, H., 1994. Frequency-dependent anisotropy of scalar waves in a multilayered medium. J. Seismic Explor., 3: 37-52.
- Smith, G.C. and Gidlow, P.M., 1987. Weighted stacking for rock property estimation and detection of gas. Geophys. Prosp., 35: 993-1014.
- Stanke, F.E. and Burridge, R., 1993. Spatial versus ensemble averaging for modeling wave propagation in finely layered media. J. Acoust. Soc. Am., 93: 36-41.
- Ursin, B., Ekren, B.O. and Tjaland, E., 1996. Linearized elastic parameter sections. Geophys. Prosp., 44: 427-455.
- Ursin, B., 1987. The plane-wave reflection and transmission response of a vertically inhomogeneous acoustic medium. In: Bernabini, M., Carrion, P., Jacovitti, G., Rocca, F., Treitel, S. and Worthington, M. (Eds.), Deconvolution and Inversion. Blackwell Scientific Publications, Oxford, pp. 189-207.
- van Geloven, W.J.F. and Wapenaar, C.P.A., 1997. Elastic imaging in finely layered media. Expanded Abstr., 67th Ann. Internat. SEG Mtg., Dallas, in press.
- van Wijngaarden, A.J. and Berkhout, A.J., 1996. Resolution analysis on AVO attributes. Expanded Abstr., 66th Ann. Internat. SEG Mtg., Denver: 1711-1714.
- Verschuur, D.J., Berkhout, A.J. and Wapenaar, C.P.A., 1992. Adaptive surface-related multiple elimination. Geophysics, 57: 1166-1177.
- Wapenaar, C.P.A. and Herrmann, F.J., 1993. True amplitude migration taking fine-layering into account. Expanded Abstr., 63rd Ann. Internat. SEG Mtg., Washington D.C.: 653-656.
- Wapenaar, C.P.A., van der Leij, T.S. and van Wijngaarden, A.J., 1995. AVA and the effects of interference. Expanded Abstr., 65th Ann. Internat. SEG Mtg., Houston: 1125-1128.
- Wapenaar, C.P.A., 1996. One-way representations of seismic data. Geophys. J. Int., 127: 178-188.
- Wapenaar, C.P.A., 1997. Amplitude-versus-angle behaviour of self-similar interfaces. Submitted to Geophysics.
- Widmaier, M.T., Shapiro, S.A. and Hubral, P., 1996. AVO correction for scalar waves in the case of a thinly layered reflector overburden. Geophysics, 61: 520-528.